JACS
JOURNAL OF THE AMERICAN CHEMICAL SOCIETY

ARTICLE

pubs.acs.org/JACS

Origin and Activity of Gold Nanoparticles as Aerobic Oxidation Catalysts in Aqueous Solution

Cheng Shang and Zhi-Pan Liu*

Shanghai Key Laboratory of Molecular Catalysis and Innovative Materials, Department of Chemistry, Key Laboratory for Computational Physical Sciences (Ministry of Education), Fudan University, Shanghai 200433, China

Supporting Information

ABSTRACT: Whether gold is catalytically active on its own has been hotly debated since the discovery of gold-based catalysis in the 1980s. One of the central controversies is on the O_2 activation mechanism. This work, by investigating aerobic phenylethanol oxidation on gold nanoparticles in aqueous solution, demonstrates that gold nanoparticles are capable to activate O_2 at the solid−liquid interface. Extensive density functional theory (DFT) calculations combined with the periodic continuum solvation model have been utilized to provide a complete reaction network of aerobic alcohol oxidation. We show that the adsorption of O_2 is very sensitive to the environment: the presence of water can double the O_2 adsorption energy to ∼0.4 eV at commonly available edge sites of nanoparticles (∼4 nm) because of its strongly polarized nature in adsorption. In alcohol oxidation, the hydroxyl bond of alcohol can break only with the help of an external base at ambient conditions, while the consequent α-C—H bond breaking occurs on pure Au, both on edges and terraces, with a reaction barrier of 0.7 eV, which is the rate-determining step. The surface H from the α-C—H bond cleavage can be easily removed by O_2 and OOH via a H_2O_2 pathway without involving atomic O. We find that Au particles become negatively charged at the steady state because of a facile proton-shift equilibrium on surface, OOH + OH ↔ O_2 + H_2O. The theoretical results are utilized to rationalize experimental findings and provide a firm basis for utilizing nanoparticle gold as aerobic oxidation catalysts in aqueous surroundings.

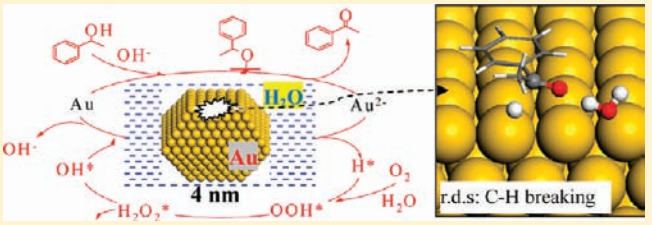

1. INTRODUCTION

It has been a consistent goal to realize homogeneous organic reactions at mild environmentally friendly reaction conditions. Solid−liquid heterogeneous catalysis as an attractive synthetic approach has been tested, and recent research demonstrated the possibility of utilizing a gold-based catalyst for the aerobic oxidation of certain alcohols to aldehydes/ketones at ambient conditions.[1−5] High activity was reported for unsupported and supported gold nanoparticles (on various inert supports such as activated-carbon, polymers, and SiO_2) in the presence of base additives and solvent (e.g., water).[6−11] The phenomenon of molecular O_2 activation on Au itself is not anticipated, as the active oxide supports (e.g., TiO_2, CeO_2) are often essential in Au-based catalysts for coactivating O_2 at solid−gas reaction conditions.[12−14] Compared to the surface reaction in ultrahigh vacuum (UHV), reactions at the solid−liquid interface are much more poorly understood, not least because of the added complexity of the solvent environment. To date, a theoretical framework is highly desired to understand the solid−liquid catalysis at the level of detail rivaling that of surface reactions in UHV, which is essential toward the rational design of improved catalysts with high activity and selectivity.

Although the detailed mechanism is still in much debate, it was now generally regarded that aerobic alcohol oxidation can be decomposed into four major steps following a Langmuir−Hinshelwood mechanism, namely, (i) the adsorption of reactants (alcohol, O_2), (ii) and (iii) the hydroxyl (OH) bond and the α-C—H bond breaking of alcohol, and finally (iv) the removal of H by O_2 or its derivatives (possibly atomic O).[15−17] As a key feature, aerobic alcohol oxidation is not very sensitive to the type of oxide supports provided with the base additives (often within 2-fold difference in activity),[18−20] unlike the well-studied CO oxidation over gold-based catalysts (e.g., 3 orders of magnitude difference in activity reported for Au/TiO_2 and Au/SiO_2).[13,21] For instance, Au/TiO_2 is a poor catalyst for alcohol oxidation in the absence of a base[19] (TiO_2 surfaces are acidic[22]), but it can catalyze CO oxidation even at low temperatures (200 K).[13] Since O_2 adsorption and activation are shown to be facile in the Au/TiO_2 system,[23] it was naturally expected that the role of the base is to enhance the decomposition of alcohol at steps (ii) and (iii), not related to O_2 reduction. A number of experimental findings indeed confirm this.[15,17,19,24,25] With isotope labeling during alcohol oxidation on Au/CeO_2, Conte et al.[17] detected the existence of Au−H species with electron paramagnetic resonance spectroscopy. They further demonstrated that the surface hydrogen is produced from the rate-determining step, the α-C—H cleavage of alcohol.[15] By direct utilizing basic oxide supports (Hydrotalcite), Mitsudome et al. showed that alcohols can still be oxidized efficiently without adding an external base.[19]

Received: April 14, 2011
Published: May 24, 2011

On the other hand, the mechanism for the O_2 reduction involving steps (i) and (iv) remains elusive. Previous work generally showed that O_2 adsorption and dissociation is kinetically difficult on pure Au at ambient conditions,[23,26−28] which is apparently contradictory to the observation on the facile O_2 reduction over different supporting materials in aerobic alcohol oxidation. Furthermore, since the working Au catalysts are usually in the form of nanoparticles at the size of a few nanometers (e.g., 5 nm in diameter, >1000 Au atoms), it is unlikely that extremely low coordinated Au corner sites (e.g., apex or adatoms) are responsible for catalyzing O_2 reduction (if so, O_2 activation would be rate-determining due to extremely low concentration of such sites). In fact, Abad et al.[15] found that the rate of alcohol oxidation increases with the increase of the area of exposed Au sites in Au/TiO_2, implying the irrelevance of the minority sites in the rate-determining step. The O_2 reduction on Au must therefore be related to the unique reaction conditions of alcohol oxidation, for example, the presence of the solid−solution interface, the participation of the base, and the possible presence of charged (anionic) Au particles.[7,8,29−31]

Using aerobic 1-phenylethanol oxidation as the model reaction, here we aim to establish a complete mechanism for this solid−liquid reaction process to answer the above puzzles. Large-scale density functional theory (DFT) calculations are performed to model the catalytically most relevant Au particles, 2−5 nm in diameter, and a periodic continuum solvation model as developed recently[32−34] was utilized to take into account the long-range electrostatic solvation effect of aqueous surroundings. We demonstrate that O_2 reduction in the presence of surface H can occur facilely on commonly available edge sites of Au particles. Not the Au coordination number, but the size of the particle and the aqueous environment are critical to O_2 adsorption and activation. The comprehensive reaction network of aerobic 1-phenylethanol oxidation is revealed, with particular emphasis on the promotional role of base and the structure-insensitivity of the rate-determining α-CH bond breaking step.

2. CALCULATION METHODS AND MODELS

All total energy calculations were performed using the DFT package SIESTA with numerical atomic orbital basis sets and Troullier−Martins normconserving pseudopotentials.[35−37] The exchange−correlation functional utilized was at the generalized gradient approximation level, known as GGA-PBE.[38] Except for Au where extra 7s polarization orbital was added for all surface atoms of gold particle, the optimized double-ζ plus polarization basis (DZP) set was employed for all elements.[37,39,40] The energy cutoff for the real space grid used to represent the density was set as 150 Ry. The basis set superposition error (BSSE) was corrected in computing the adsorption energy (E_{ad}) of molecules. The vibrational frequency of reaction intermediates was calculated by the numerical finite-difference method, and the results were then utilized to correct the zero point energy (ZPE). The geometry relaxation was carried out using the quasi-Newton Broyden method until the maximal force on each coordinate is below 0.1 eV/Å for all surface reactions and a finer criterion (<0.05 eV/Å) for computing adsorption energetics. The transition states (TS's) of the reactions were searched using our recently developed constrained-Broyden-minimization method[41] and constrained-Broyden-dimer method.[42] For the extended Au surfaces, a $p(3 \times 2\sqrt{3})$ (8.824 × 10.190 Å) and $p(1 \times 5)$ (12.128 × 14.707 Å) four layer slabs were used for (111) and stepped (322) surfaces, respectively, with the bottom two layers fixed at the bulk-truncated position (see Figure S1 of the Supporting Information for the structure of the (322) surface, which has a monatomic (100) step every four rows of (111) terrace). The Monkhorst−Pack k-points sampling of (2 × 2 × 1) and (1 × 3 × 1) were utilized for the two surfaces. A convergence check of the above calculation setups have been checked by benchmarking the O_2 adsorption energetics on extended Au surfaces with the plane-wave basis-set codes, which showed that the difference in adsorption energetics is within 0.05 eV.

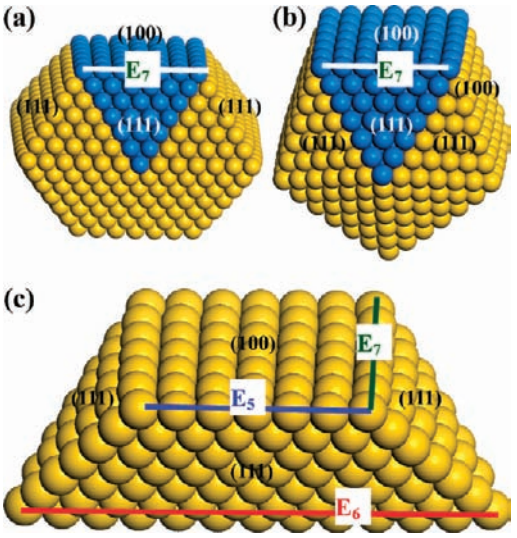

Figure 1. Model of Au nanoparticles. (a) decahedral gold cluster; (b) penta-star gold cluster; and (c) a Au_{252} cluster that is a common building block (shaded by blue color in a and b) for decahedral and penta-star clusters. Edge sites, including E_5, E_6, and E_7, are labeled.

Without explicit mention, the long-range electrostatic solvation effect for the catalytic systems in aqueous surroundings has always been taken into account by using a periodic continuum solvation model based on the modified Poisson−Boltzmann equation (CM-MPB).[32−34] The details on the implementation of the CM-MPB model are also given in the Supporting Information. Explicit water molecules have also been considered to examine the possible specific interaction between the first-shell water and the reaction intermediates. Compared to that of small molecules, the solvation effect of solid surfaces is more challenging to measure or compute due to the dynamic metal−solution interface structure. To validate our model on treating the Au surface, we have calculated the potential of zero charge (PZC) of Au(111) surface using the CM-MPB approach and it gives 0.32 V versus standard hydrogen electrode, in a fair agreement with experimental values, ∼0.5 V.[43] It should be mentioned that the computed solvation energy gain for Au surfaces with CM-MPB is generally low, that is, 0.028, 0.035, and 0.042 eV per surface Au atom for Au(111), (100), and (322) surfaces, respectively, indicating that the solvation effect on reactions, if present, should mainly act on the polarized reaction intermediates.

To compute the adsorption energy (E_{ad}) of a species X in solution, we utilize eq 1

$$E_{ad}(X) = E_{tot}(Au) + E_{tot}(X) - E_{tot}(X/Au) \quad (1)$$

where E_{tot} is the DFT total energy in aqueous solution (via the CM-MPB model), respectively. The larger (more positive) the value is, the more strongly the species binds on surface. Similarly, the adsorption energy for the species X without solvent can be calculated by directly using the DFT total energy in vacuum (without the CM-MPB model) on the right-hand side of eq 1.

2.1. Models of Gold Nanoparticles. To investigate the catalytic reactions on gold nanoparticles, we have constructed a series of gold nanoparticles from ∼2 to ∼5 nm by only exposing the lowest surface energy (111) and (100) microfacets according to Wulff construction rule,[44,45] namely, three decahedral gold clusters, Au_{203}, Au_{429}, and Au_{781} (surface area (111):(100) = $3(3)^{1/2}$:1), and a penta-star gold cluster Au_{932} (surface area (111)/(100) = $3^{1/2}$:2), as shown in Figure 1a and b.

dx.doi.org/10.1021/ja203468v | J. Am. Chem. Soc. 2011, 133, 9938–9947

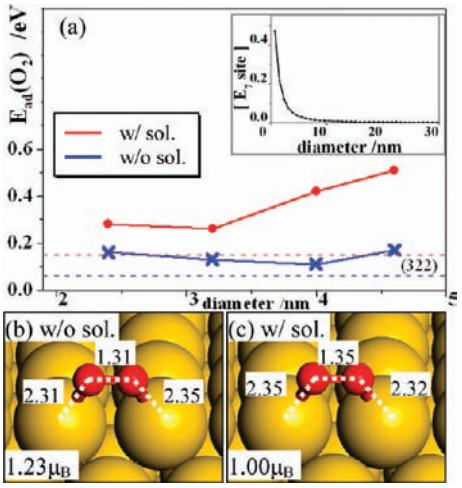

Figure 2. O_2 adsorption on Au nanoparticles in the presence (w/sol.) or absence (w/o sol.) of aqueous solution. (a) The adsorption energy of O_2 ($E_{ad}(O_2)$) at E_7 sites of clusters, Au_{203}, Au_{429}, Au_{781}, and Au_{932}. Dashed lines represent the values of $E_{ad}(O_2)$ on stepped Au(322) with and without solvent. The insert shows the rapid drop of the population of E_7 sites ([E_7 site]) with the increase of particle diameter. (b and c) The optimized structure for O_2 adsorption on the E_7 site of Au_{781}. The key distances (Å) and spin polarization (μ_B) of the adsorbed oxygen molecules are indicated.

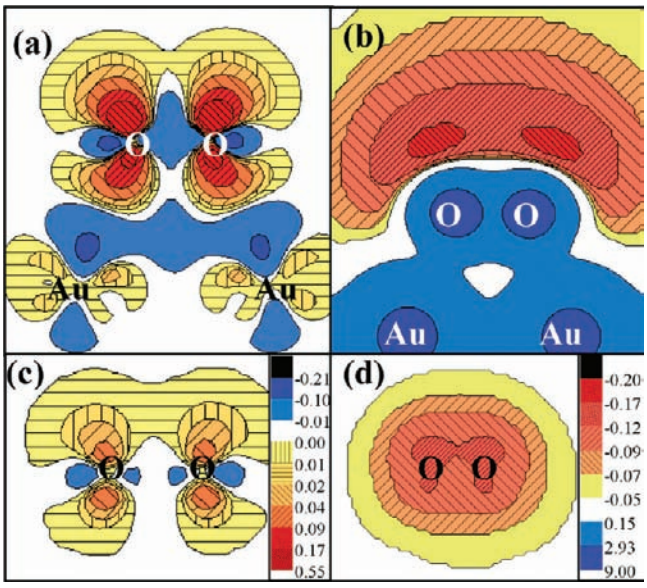

Figure 3. (a) The contour plot for the total electron charge density difference (unit: e/Å^3) before and after and O_2 adsorption on Au nanoparticle in solution, constructed by subtracting the total electron densities of the O_2 adsorbed model (O_2/Au) from the separated O_2 and Au cluster. (b) The contour plot of total electrostatic potential (unit: V) for the O_2 adsorbed system in solution. (c) The change of the total electron charge density difference induced by solvation. (d) The change of the total electrostatic potential induced by solvation. All contour planes are cutting through the bonding plans of O_2 with Au.

The similar nano gold structures have been observed experimentally or used in previous theoretical calculations.[46−48] From our calculations, the surface energies of the (111) and (100) of Au are close (different by 0.14 J/m^2) in aqueous surroundings, and therefore the exact morphology of Au particles [(111):(100) ratio] can be sensitive to the synthetic conditions as has been explored in the experiment.[49−51] The details for computing the surface energy are given in the Supporting Information.

For chemical reactions, the local surface sites ought to receive more attention, where the available bonding geometry and the Au coordination number (a simple index often utilized to indicate the saturation level of Au atom) often dictate the activity. It can be seen from Figure 1a that the corner and apex sites (the Au coordination number below four) have a very low population (<0.06%) on all Wulff particles, and we therefore only considered the terrace sites and the edge sites as the possible active sites for aerobic alcohol oxidation. From a theoretical point view, the terrace/stepped sites may be represented by extended surfaces in slab calculations using crystalline surfaces, such as (111), (100) ,and (322) as also utilized in this work. On the other hand, the edge sites that are common to nanoparticles are often not present on low Miller index surfaces and thus rarely investigated previously due to the high computational demanding of nanoparticle systems. This kind of edge sites commonly available in nanoparticles, denoted as E_7 sites, is located at the conjunction between (111) and (100) surfaces with an obtuse dihedral angle (120° from bulk-truncated structure). The Au coordination number of E_7 sites is seven, two less than that of surface atoms on the close-packed (111). These unique sites should therefore be the focus for investigating the catalytic properties of nanoparticles.

3. RESULTS

3.1. O_2 Adsorption and Dissociation on Au Nanoparticles in Aqueous Solution. To fully understand the O_2 reduction process on gold, it is important to determine the O_2 adsorption energy ($E_{ad}(O_2)$) on gold nanoparticles and assess the possible effects due to the finite size of particle. The Au clusters studied, including three decahedral Au_{203}, Au_{429}, and Au_{781} and a pentastar Au_{932} (see calculation models for detail), vary from 2 to 5 nm in diameter, which are in the regime most relevant to the oxidation reactions on gold.[52−54] As mentioned, we will mainly focus on the O_2 adsorption on the commonly available E_7 sites of these nanoparticles, and the results are compared to those on extended (111) and stepped (322) surfaces. The calculated results are plotted in Figure 2a. As a representative, the optimized structures for adsorbed O_2 on Au_{781} are shown in Figure 2b.

Figure 2 shows that $E_{ad}(O_2)$ with solvent (red curve) is generally larger than it without solvent (blue curve) at the E_7 sites of Au particles. In the presence of water, $E_{ad}(O_2)$ is 0.3 eV on a 2 nm Au_{203} cluster, and it can reach to 0.4−0.5 eV on 4−5 nm Au clusters, where the solvation effect could contribute more than the half, ~0.3 eV. $E_{ad}(O_2)$ without solvent is consistently low, being around 0.1 eV. Consistently, the spin polarization for adsorbed oxygen with solvent is generally lower compared to that without solvent, as shown in Figure 2b,c, which implies that O_2 is more negatively charged in solution. For comparison, $E_{ad}(O_2)$ on extended surfaces without or with solvent are also computed and found to be below 0.2 eV, no matter whether close-packed (111) (0.05/0.13 eV) or stepped (322) (0.07/0.15 eV, shown by the dotted lines in Figure 2a). These low values should represent the limit for O_2 adsorption on large (bulk-like) Au particles and therefore confirm the nobleness of bulky Au, even in aqueous solution. Contrary to the conventional view, $E_{ad}(O_2)$ is not sensitive to the Au coordination number, considering that the Au atoms involved in O_2 adsorption on Au(322) (steps) and nanoparticles (E_7 site) are both seven coordination but $E_{ad}(O_2)$ values are distinct. From these results, we can conclude that both the finite size of the particle and the water surroundings are important to O_2 adsorption on Au.

It should be emphasized that the concentration of E_7 sites decreases rapidly with the increase of the particle size. Their

dx.doi.org/10.1021/ja203468v |J. Am. Chem. Soc. 2011, 133, 9938–9947

relation in the decahedron Wulff particle is plotted in the insert of Figure 2a, from which we can estimate that the concentration of E_7 site in 10 nm Au clusters is already 1 order of magnitude lower than that in 2 nm Au clusters. The Au nanoparticle size below 4 nm is therefore predicted to be the optimum size regime, which possesses both a high concentration of E_7 sites (>5.1%) and a reasonable O_2 adsorption energy, that is, 0.3−0.4 eV.

To provide deeper insight into the remarkable solvation effect for O_2 adsorption, we have examined the electronic structure of the O_2 adsorbed Au_{781} system with and without the solvation by analyzing the total electronic charge density and the total electrostatic potential. In Figure 3a, we have shown the contour plot for the total electronic charge density difference before and after the O_2 adsorption on the Au cluster in solution, which is constructed by subtracting the total electron densities of the O_2 adsorbed model (O_2/Au) from the separated O_2 and Au cluster. The contour plane is cutting through the bonding plans of O_2 with Au. It shows that the $2\pi^*$ of O_2 can bond with the d_{z2} orbital of gold with the net electron flow from Au to O_2 (adsorbed O_2 is −0.52 charged from Mulliken analysis). To be consistent with this picture, the total electrostatic potential for the O_2 adsorbed system in solution, shown in Figure 3b, also demonstrates the strong polarized nature of O_2/Au. The negative electrostatic potential is located maximally at the $2\pi^*$ lobes of O_2 distal to the surface.

The solvation effect can then be visualized by plotting the change of the total electronic charge density difference and the total electrostatic potential on going from the vacuum model to the solvation model, as shown in Figure 3c and d, respectively. We found that the solvation can induce extra electron accumulation on O_2 $2\pi^*$ orbital, but the electron depletion is not localized on the Au atoms in contact with O_2, indicating a nonlocal electron donation behavior of Au and the internal polarization of the whole Au particle. Fundamentally, the electron density relocation in Figure 3c can be rationalized by the applied external solvation potential shown in Figure 3d, which places a net negative electrostatic field centered on the adsorbed O_2 molecule. It is the intrinsic polarization of O_2 binding on Au that facilitates the subsequent solvation energy gain at the Au/O_2/solution interface.

To efficiently map out the reaction network in aerobic alcohol oxidation, we have considered utilizing a truncated Au cluster model to represent the active E_7 site based on two facts: the E_7 site being the junction between (111) and (100) facets is commonly available and $E_{ad}(O_2)$ is rather constant (0.3−0.4 eV) for Au nanoparticles below 4 nm in solution. The model we adopted is an Au_{252} cluster, which is a common building block for the decahedral gold cluster and the penta-star gold cluster, as shown in Figure 1. The structure stability of the Au_{252} cluster has been checked by fully optimizing the structure of the cluster until the maximal force on each coordinate is below 0.01 eV/Å. The length of E_7 in the optimized Au_{252} cluster is 16.68 Å, which is 5.25% squeezed with respect to the bulk-truncated structure. The dihedral angle between (111) and (100) surfaces was 128° (120° in the bulk-truncated structure). As will be shown below, we found that the commonly available E_7 sites of Au nanoparticles, as represented by those in Au_{252}, are already capable to catalyze the aerobic alcohol oxidation.

On the Au_{252} cluster model, we have explored the possible adsorption sites for O_2, including the (111) and (100) terrace sites, namely, $T_{(111)}$ and $T_{(100)}$, and three types of edges, namely E_5, E_6, and E_7 (the number in subscript indicates the coordination number of the edge Au). All of the results are shown in Table 1. As expected, $E_{ad}(O_2)$ without solvent is weak (<0.18 eV) on all sites despite the small size of the cluster. This is consistent with previous calculations and experimental findings on various Au surfaces.[26,55,56]

Table 1. O_2 Adsorption and Dissociation on the Au_{252} Cluster

	$T_{(100)}$	$T_{(111)}$	E_5	E_6	E_7
CN(Au)[a]	8	9	5	6	7
$E_{ad}(O_2)$ (eV) (w/o sol.)	0.00	0.08	0.11	0.15	0.18
$E_{ad}(O_2)$ (eV) (w sol.)	0.17	0.26	0.41	0.32	0.37 (0.38[b])
d_{O-O} (Å)	1.32	1.28	1.35	1.35	1.33
spin (μ_B)	1.24	1.69	1.01	1.02	1.06
$E_a(O_2 \rightarrow 2O)$ (eV)			1.28	1.32	1.47

[a] Coordination number of Au. [b] With two explicit water molecules as the first solvation shell.

Similar to the results on the Wulff particle models, we found that the aqueous surroundings can improve $E_{ad}(O_2)$ by ∼0.2 eV on the Au_{252} and O_2 adsorbs most strongly at the edge sites and there is no obvious preference in adsorption among E_5, E_6, and E_7 sites despite the difference in their coordination number. The calculated spin polarization of the adsorbed oxygen at these edge sites are also very similar, being around 1.0 μ_B, consistent with that found in the decahedral Au_{781} (Figure 1c). At the E_7 sites, $E_{ad}(O_2)$ increases from 0.17 eV without solvent to 0.37 eV with solvent, a value indeed within the window of $E_{ad}(O_2)$ in solution for 2−4 nm Wulff particles (Figure 1a). It might be mentioned that we also checked $E_{ad}(O_2)$ at the E_7 site by further adding two explicit water molecules as the first solvation shell to take into account the possible short-range specific interaction (the continuum solvation is always applied in background), and the recalculated value is 0.38 eV, indicating that the continuum solvation model is already enough to describe the energetics for O_2 adsorption in aqueous surroundings.

Next, we also considered the possible effect of solute, that is, the added base, on the O_2 adsorption. This required us first to determine the most likely adsorption site of the OH anion on Au. The OH anion in water has a large free energy of solvation ($\Delta G_{sol}(OH^-)$ defined by the free energy change of $OH^- + (H_2O)_n \rightarrow OH^-(H_2O)_n$), and thus the adsorption of OH anion is governed by the free energy change $\Delta G_{ad}(OH^-)$ for the OH anion moving from solution to the surface. (The details for calculating $\Delta G_{ad}(OH^-)$ are given in the Supporting Information.) Using the reported experimental value $\Delta G_{sol}(OH^-) = -4.6$ eV as the reference[57,58] (our calculated value is −4.53 eV ($n = 4$) with the CM-MPB model), we found that $\Delta G_{ad}(OH^-)$ is low on terrace sites, 0.04 and 0.04 on $T_{(100)}$ and $T_{(111)}$ terrace sites, respectively, but increases to 0.50, 0.51, and 0.52 eV on E_5, E_6, and E_7 sites, respectively. On all of the edges, the OH anion sits at a bridge site bonding with two edge Au atoms. Obviously, the coadsorption of OH anion and O_2 at the edge sites is thermodynamically most likely to occur since both species prefer to adsorb at the edge sites. Our calculations show that adsorbed OH and O_2 are repulsive by 0.21 eV in coadsorption, which is attributed to the fact that both OH and O_2 are electronegative adsorbates. This result rules out the direct involvement of OH in promoting O_2 adsorption.

It should also be mentioned that the dissociation of O_2 to atomic O on the Au cluster were found to be infeasible at ambient conditions. Our calculated O_2 dissociation barrier at the edges

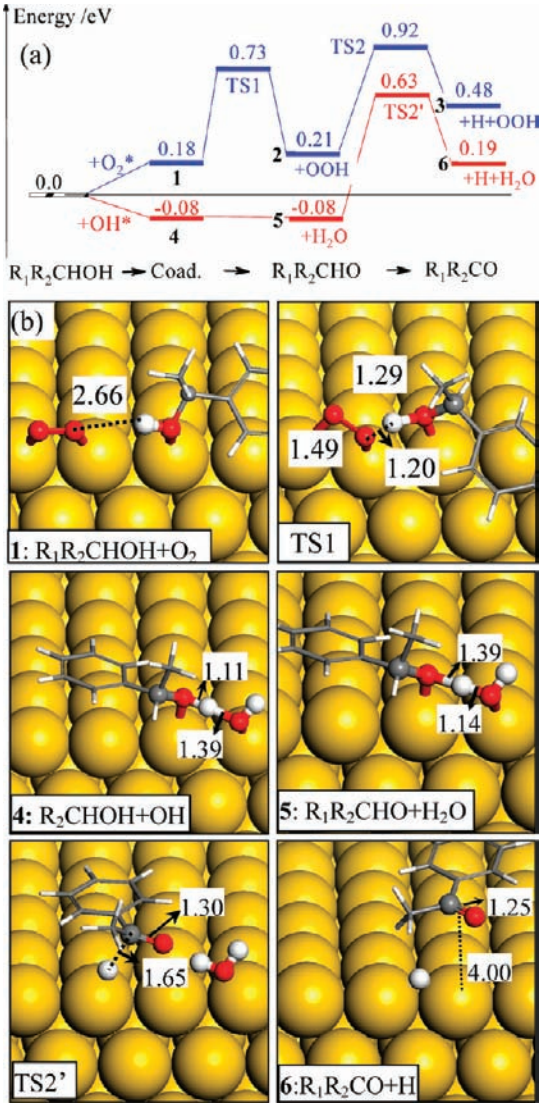

Figure 4. (a) Potential energy diagram (ZPE-corrected) of the reaction channels for 1-phenylethanol oxidation in the absence (blue) and presence (red) of base (OH). The energy zero is defined as the individual adsorption state of O_2, phenylethanol, H_2O, and OH (see Table 2). (b) Snapshots of key reaction intermediates and the TS's: R_1=Ph and R_2=CH_3. Apart from an additional individually adsorbed OOH species (see Figure 5), the state of **2**, **3**, and TS2 in the O_2-assisted pathway are the same with the state of **5**, **6**, and TS2′ in the OH-assisted pathway, respectively. The key distances (Å) are indicated.

without solvent is extremely high, more than 2 eV. In the aqueous surroundings, although the solvation can help to reduce the barrier, the calculated barriers at Au edges are still above 1 eV in general (see Table 1 and Figure S2 of the Supporting Information for the TS structure). Comparing to the low O_2 adsorption energy (~0.4 eV), O_2 would prefer to desorb rather than dissociate on Au kinetically. In other words, the residence time for O_2 on Au is too short to dissociate at the ambient conditions. It is therefore expected that the O_2 reduction is not via the O_2 direct dissociation channel (i.e., via atomic O).

3.2. Reaction Network for Phenylethanol Oxidation on Au. To map out the whole reaction network, we took a recursive "trial-and-error" approach, the high work load of which is largely eased by the recently developed constrained TS location techniques.[41,42] We first explored the initial bond cleavage of 1-phenylethanol by breaking its CH or OH bond individually and then walked through each "likely" oxidation channel stepwise until acetophenone were reached. By "likely", we mean that the reaction route must have relatively low reaction barriers, typically below 0.75 eV (a magnitude regarded as surmountable for surface reactions occurring at room temperatures). In deducing a complete oxidation mechanism, we also took into account the participation of base (adsorbed OH) and molecular O_2 in reactions, which can serve as oxidants to accept H. In the following section, we elaborate on our calculated reaction network, including 1-phenylethanol oxidation to acetophenone and the O_2 reduction on the Au_{252} cluster.

Table 2. Calculated Adsorption Energy (eV) of Key Reaction Intermediates on the E_7 Edge Site of the Au_{252} Cluster without and with Solvent (via the CM-MPB Model)[a]

	w/o solvent		w/solvent			
species	(111)	E_7	(111)	E_7	$\Delta E_{ad(sol)}$[b]	d_{Au-X}[c] (Å)
O_2	0.05	0.18	0.13	0.37	0.24	2.40
1-phenylethanol	0.34	0.42	0.10	0.46	0.36	2.51
H	−0.28	−0.05	−0.31	−0.11	0.20	1.77
1-phenylethoxy	1.31	1.37	1.18	1.32	0.14	2.15
acetophenone	0.06	0.20	−0.12	0.13	0.25	2.42
H_2O	0.15	0.20	−0.01	0.19	0.20	2.71
OOH	0.62	0.76	0.50	0.89	0.39	2.22
OH	2.14	2.48	2.12	2.45	0.32	2.32
O	−0.10	0.04	0.09	0.28	0.19	2.12

[a] For comparison, the values on the extended (111) surface are also listed. All adsorption energies are calculated using eq 1 (for H and O atoms, the adsorption energy is with respect to 1/2 H_2 and 1/2 O_2, respectively). [b] $\Delta E_{ad(sol)}$ is the adsorption energy difference between at the E_7 site and at the extended (111) sites in solution. [c] d_{Au-X} is the shortest distance between Au and the adsorbate at the E_7 edge site of Au_{252} cluster with solvent. Except for H (X = H), all the other adsorbates bond with Au via their O end (X = O).

3.2.1. Phenylethanol Oxidation to Acetophenone. The phenylethanol dehydrogenation can follow either a direct mechanism (on Au) or an indirect mechanism assisted by the reactant O_2 or the promoter OH anion. In Figure 4a, we show the determined energy profile (ZPE-corrected) for the most favorable reaction channels in the absence (blue curve) and presence (red curve) of base, which are named as the O_2-assisted pathway and the OH-assisted pathway, respectively, depending on how the first hydrogen is removed from phenylethanol. In both pathways, the OH bond of phenylethanol breaks first which is followed by the α-CH bond breaking of phenylethoxy. The other possible reaction channels (e.g., first, the CH-bond breaking and then the OH-bond breaking) are less favorable and thus will be only mentioned briefly. The optimized key reaction intermediates and the TS's are shown in Figure 4b.

The adsorption energy of the involved reaction intermediates have been calculated in solution using eq 1 and are listed in Table 2. It shows that all reaction intermediates, not only molecular O_2, prefer to adsorb at the edge sites of Au particle compared to the (111) surface. The magnitude of the preference varies from 0.14 to 0.39 eV: 1-phenylethoxy has the flattest potential energy surface, while OOH, OH, and 1-phenylethanol have the most corrugated potential energy surface. We also

dx.doi.org/10.1021/ja203468v | J. Am. Chem. Soc. 2011, 133, 9938–9947

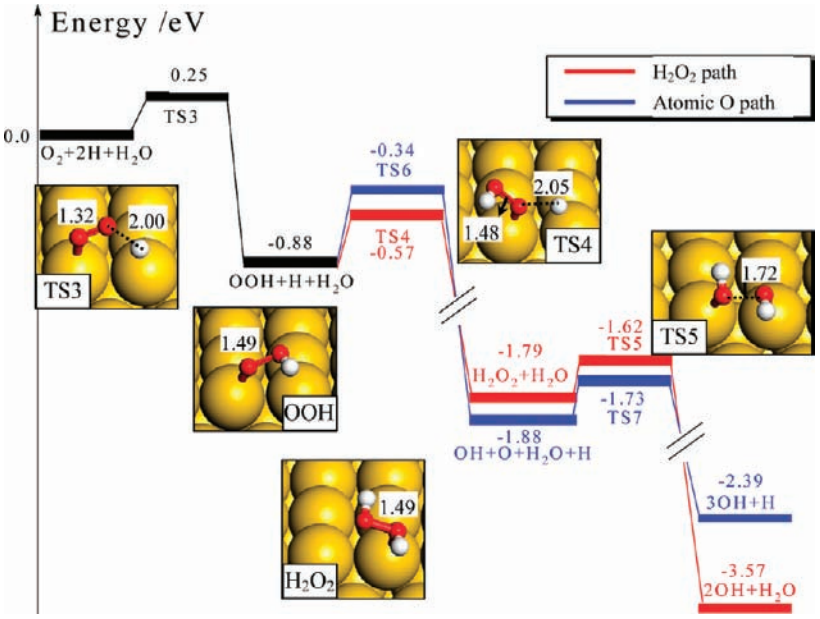

Figure 5. Potential energy diagram (ZPE-corrected) of O_2 reduction by surface H. The energy zero is defined as the individual adsorption state of O_2, H, and H_2O (see Table 2). The key reaction intermediates and the TS's are also shown. The key distances (Å) are indicated.

noticed that the presence of aqueous solution can enhance greatly the adsorption of O_2-derivatives, including O_2, O atom (>0.2 eV), and OOH (0.13 eV), apparently due to their large electronegativity. It might be mentioned that the adsorption data in solution listed in Table 2 are with the implicit solvation model only. The explicit H_2O molecules have been added in calculating reaction profiles. For example, 1-phenylethoxy has a large coadsorption energy gain with an explicit H_2O (0.39 eV) due to the formation of a strong H-bonding.

O_2-Assisted Pathway. In this pathway, the adsorbed phenylethanol first breaks its hydroxyl bond and passes the H to a neighboring adsorbed O_2, which yields a 1-phenylethoxy and an OOH. At the initial state (IS, state **1**), the coadsorption of O_2 and phenylethanol is repulsive by 0.18 eV. At the TS (TS1), the passing H is far away (2.65 Å) from the surface Au but sits in between two O atoms with a short distance (1.20, 1.29 Å), implying that this is a proton transfer process (see Figure 4). The newly formed 1-phenylethoxy (state **2**) adsorbs also most strongly at the edge site (see Table 2), and it can form a strong H-bonding interaction with a neighboring (explicit) water molecule (Figure 4b) with the coadsorption energy gain being 0.39 eV. Next, the 1-phenylethoxy breaks the α-CH bond over an edge Au atom to produce an acetophenone (state **3**) that can readily desorb from the surface (E_{ad}(acetophenone) is only 0.13 eV). At the TS of the α-CH bond breaking (TS2), the C−H bond is stretched to 1.65 Å, and the evolving acetophenone is floating over the Au surface with the C−Au distance being at least 3.2 Å; the calculated reaction barrier (E_a) is 0.71 eV. It might be mentioned that the presence of the explicit water is essential to calculate the barrier of α-CH breaking step due to the large coadsorption energy gain at the IS (with only the implicit solvation, the α-CH breaking barrier is 0.34 eV). Overall, the O_2-assisted pathway produces acetophenone and adsorbed surface H and OOH, and the reaction energy (ΔH) is +0.48 eV (endothermic). The overall barrier height is 0.92 eV (the energy difference between TS2 and the initial adsorbed phenylethanol), which is a sum due to both the α-CH and the hydroxyl bond breaking.

It might be mentioned that the other possible channels for the first dehydrogenation of phenylethanol are unlikely to occur due to their higher barriers (>1.2 eV). These unfavorable channels include the direct hydroxyl bond breaking ($R_1R_2CHOH \rightarrow H + R_1R_2CHO$, R_1=Ph, and R_2=CH_3; hereafter, E_a = 1.67 eV and ΔH = 1.49 eV), the direct α-CH bond breaking ($R_1R_2CHOH \rightarrow H + R_1R_2COH$; E_a = 1.69 eV and ΔH = 1.12 eV), and the O_2-assisted α-CH bond breaking ($O_2 + R_1R_2CHOH \rightarrow OOH + R_1R_2COH$; E_a = 1.31 eV and ΔH = 0.24 eV).

OH-Assisted Pathway. In the presence of the OH anion that adsorbs at the edge site, the adsorbed phenylethanol can readily lose its H of the hydroxyl group to the neighboring OH. The coadsorption of OH and phenylethanol is attractive by 0.08 eV (state **4**), and the distance between the H of phenylethanol and the OH only 1.3 Å at the IS. Due to the close contact of the two species, the consequent proton transfer is essentially barrierless, which finally yields a 1-phenylethoxy and an H_2O (state **5**). The next step, α-CH bond breaking, is the same as that in the O_2-assisted pathway with a barrier of 0.71 eV. In this pathway, an acetophenone is formed together with a surface H and a water molecule (state **6**). The overall barrier height in the OH-assisted pathway is thus 0.71 eV, originated solely from the α-CH breaking step.

It is interesting to notice that the presence of base, or more generally the electronegative species, does not help the α-CH bond breaking of phenylethoxy. We have utilized O_2, OH, or OOH as the H acceptor to assist the α-CH dissociation, and the calculated barriers are all higher than 1 eV ($O_2 + R_1R_2CHO \rightarrow OOH + R_1R_2CO$: E_a = 1.08 eV and ΔH = −0.62 eV; $OH + R_1R_2CHO \rightarrow H_2O + R_1R_2CO$: E_a = 1.09 eV and ΔH = −0.90 eV; $OOH + R_1R_2CHO \rightarrow H_2O_2 + R_1R_2CO$: E_a =1.21 eV and ΔH = −1.79 eV). This is consistent with the fact that the H on α-C is not proton-like (calculated Mulliken charge of H is +0.02, in comparison with +0.34 of H in hydroxyl of phenylethanol) and the CH bond breaking cannot be promoted by the electronegative acceptor.

From the reaction profile in Figure 4a, we can finally summarize three key features in the phenylethanol decomposition: (i) The presence of OH can reduce the overall barrier by 0.21 eV,

dx.doi.org/10.1021/ja203468v |*J. Am. Chem. Soc.* 2011, 133, 9938–9947

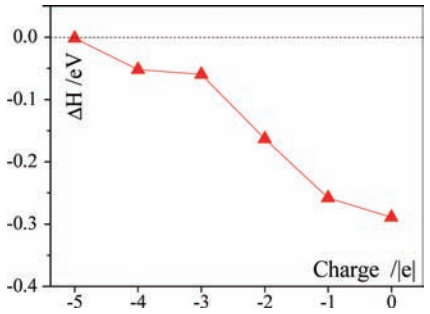

Figure 6. Reaction energy (ΔH) of OH* + OOH* → O_2* + H_2O* on differently charged Au_{252}^{n-}.

indicating the strong promotional effect of the external base. Such an energy difference would mean that the reaction rate is different by 4 orders of magnitude at 300 K, assuming the pre-exponential factors are the same. (ii) The hydroxyl bond breaking of phenylethanol must be promoted by electronegative species, either coadsorbed O_2 or OH, since the direct hydroxyl bond breaking over Au is highly activated (>1.2 eV). Obviously, the hydroxyl bond breaking is sensitive to the basicity of the H acceptor. The stronger basicity of OH compared to O_2 causes the lower overall barrier of the OH-assisted pathway. (iii) The α-CH bond breaking occurs most favorably via the direct dehydrogenation over the Au site. Therefore, no matter which pathway is involved, the surface H is always produced due to the intrinsic low barrier of α-CH bond breaking over Au. This is important as it implies that the presence of surface H on Au might be universal in alcohol oxidation on Au-based catalysts, independent of the type of oxide supports or the added base. The presence of H on Au was first confirmed by Conte et al.[17] over a Au/CeO_2 catalysts using isotope experiment, who demonstrated that the surface H originates from the α-C—H cleavage.

3.2.2. O_2 Reduction by Surface H. The OH-assisted dehydrogenation of phenylethanol consumes OH anions from the solution, produces adsorbed H and H_2O, and consequently leaves negative charges to the Au particle ($OH^- + PhCH(CH_3)OH \rightarrow PhC(CH_3)O + H_2O + H^* + e^-$, superscript * indicates the adsorbed state). To close the catalytic cycle, the reactant O_2 must be reduced to regenerate OH anion and restore the charge state of Au. Due to the presence of OH anions, we found that the O_2 reduction mechanism can be quite complex, involving several competing reaction routes. The most straightforward one is the stepwise hydrogenation via a hydrogen peroxide (H_2O_2) intermediate, namely, from O_2 to OOH, H_2O_2 and finally to the OH anion, as shown in Figure 5. These pathways are described in the following section.

H_2O_2 Pathway. While the direct dissociation of O_2 is not feasible, as addressed in Section 3.1, we found that the surface H can react with an adsorbed O_2 to form OOH with a low barrier (E_a = 0.25 eV). Next, the OOH can react with another surface H to form H_2O_2, which is followed by the cleavage of the O—O bond to produce OH. The barriers for the formation and degradation of H_2O_2 are 0.31 and 0.17 eV, respectively. The whole reaction is highly exothermic by 3.57 eV per O_2, as shown in Figure 5. The highest barrier, 0.31 eV, occurs at the OOH + H → H_2O_2 step, which is still much lower than that in the dehydrogenation of phenylethanol. Finally, the surface OH can desorb into the solution as OH anion, which removes the extra electrons on the surface that were left by the OH-assisted 1-phenylethanol oxidation.

Scheme 1. Complete Mechanism for the Aerobic Oxidation of 1-Phenylethanol[a]

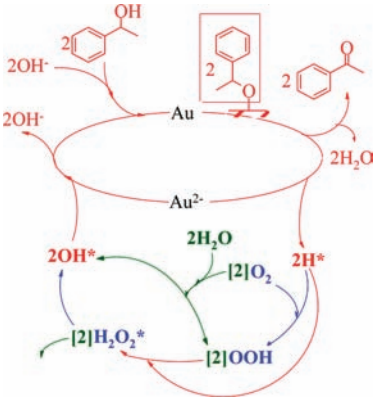

[a] The key surface intermediate, 1-phenylethoxy, is highlighted in the dotted box.

For the adsorbed H_2O_2 at the E_7 site, in parallel to its dissociation, it can also desorb by overcoming the adsorption energy, which is 0.20 eV, very close to the dissociation barrier 0.17 eV. Considering that H_2O_2 dissociation requires two surface atoms/sites at the TS (for two OHs), it is anticipated that H_2O_2 would become more likely to desorb into solution when the E_7 sites are highly populated by surface species. This is likely because all reaction intermediates prefer to adsorb at the E_7 site compared to the (111) terraces. We noticed that Zope et al.[29] reported that H_2O_2 dissociation is highly activated by 0.7 eV on Au(111), which is used to rationalize the detected H_2O_2 formation in experiment. Our results here provide an alternative view that H_2O_2 can in fact both decompose and desorb at the edge sites of Au nanoparticles with low barriers, and the production of H_2O_2 is kinetically controlled, which is sensitive to the coverage of the edge sites.

Atomic O Pathway. Alternative to the hydrogenation of OOH, OOH can also dissociate into atomic O and OH by overcoming a barrier of 0.54 eV (TS6). The atomic O can then react with a neighboring H_2O via proton exchange (TS7) to generate two OH groups (The structures of TS6 and TS7 are shown in Supporting Information Figure S2). In total, three OH groups are produced on the surface, which can end up with OH anion in solution or with H_2O by accepting the hydroxyl H from alcohol. Because the barrier height of the atomic O pathway is about 0.2 eV higher than that of the H_2O_2 pathway, the pathway is kinetically unlikely, and the atomic O will not be produced on Au surface.

It should be mentioned that we also identified a fast proton exchange equilibrium for OOH reacting with a neighboring OH,[29] that is, OH* + OOH* → O_2* + H_2O* at the E_7 site of Au (the structures are shown in Figure S2 of the Supporting Information). On the neutral Au_{252}, we found that the reaction is facile with the barrier below 0.1 eV and is exothermic by 0.29 eV. Since the OH* + OOH* → O_2* + H_2O* reaction does not involve electrons, it means that the negative charge on the Au particle would accumulate if the surface OOH keep being consumed by the adsorbed OH that is from OH anion in solution (overall reaction: $OH^-_{(sol)}$ + OOH* + Au → O_2* + H_2O* + Au^-). It is naturally expected that the accumulation of electrons should in turn quench the reaction (to the left). By gradually charging the Au cluster by additional electrons, we indeed found

dx.doi.org/10.1021/ja203468v |J. Am. Chem. Soc. 2011, 133, 9938–9947

that, as the net electrons on Au_{252} increases to 5 (Au_{252}^{5-}), the reaction becomes thermal neutral, as shown in Figure 6. This indicates that the proton-exchange equilibrium can be achieved over the anionic Au particle. At the steady state, this equilibrium provides a new channel for O_2 reduction to surface OOH with even a lower barrier compared to that of O_2 direct hydrogenation; the surface H can then be consumed by the formed OOH.

3.2.3. Complete Reaction Network. On the basis of the determined pathways, we can complete the reaction network of phenylethanol oxidation, as summarized in Scheme 1. There are seven key elementary steps in the main reaction channel numbered sequentially below from 1 to 7.

$$OH^-_{(sol)} + Au \leftrightarrow OH^* + Au^- \quad (1)$$

$$OH^* + PhCH(CH_3)OH^* \rightarrow PhC(CH_3)O + H_2O + H^* \quad (2)$$

$$H^* + O_2{}^* \rightarrow OOH^* \quad (3)$$

$$H^* + OH^* \rightarrow H_2O_2{}^* \quad (4)$$

$$H_2O_2{}^* \rightarrow 2OH^* \quad (5)$$

$$H_2O_2{}^* \rightarrow H_2O_{2(sol)} \quad (6)$$

$$OH^* + OOH^* \leftrightarrow O_2{}^* + H_2O^* \quad (7)$$

Among the steps, reaction 2, the α-CH bond breaking, is the key step that possesses the highest barrier. The absence or the presence of the base does not change the rate-determining step but will lower the overall barrier of the alcohol dehydrogenation by facilitating the hydroxyl dehydrogenation of alcohol. Obviously, the lack of catalytic ability to break the hydroxyl bond is the key problem for gold, even nanoparticles, which is the fundamental reason why the external base is often required.

The O_2 reduction mechanism is more complex as it is related to both the surface coverage and the charge state of Au particle. At the initial stage when Au is neutral and the surface coverage is low, the reaction follows 1−5 elementary steps with the decomposition of H_2O_2 on the surface (red + blue cycle in Scheme 1. Due to the presence of the side reaction 7 (on neutral Au the reaction favors the right-hand side product, O_2 and H_2O), the added base will lead to the Au particle being negatively charged gradually. Once the reaction reaches to the steady state, when the surface coverage is high and Au particles are negatively charged, another O_2 reduction channel, step (6−7), takes over, in which the adsorbed H_2O_2 desorbs and the reaction 7 $O_2{}^* + H_2O^* \rightarrow OH^* + OOH^*$ over anionic Au nanoparticles provides a facile route to reduce O_2 to OOH (red + green cycle in Scheme 1). The overall reaction thus follows a network including steps (1−4) and (6−7). Therefore, the catalytic roles of the added base are dual-fold: first, to start the reaction by facilitating the hydroxyl bond breaking of alcohol and second, to maintain the $OH^* + OOH^* \leftrightarrow O_2{}^* + H_2O^*$ equilibrium by providing the negative charges to the Au particle.

It is worth comparing our O_2 reduction mechanism with that proposed by Zope et al.[29] recently. Using Au(111) as the model, they proposed that the O_2 reduction follows $O_2{}^* + H_2O^* \rightarrow OH^* + OOH^*$ and $OOH^* + H_2O^* \rightarrow H_2O_2{}^* + OH^*$. While the former reaction is the step (7) above, also identified on the edge site of Au particles, we noticed that the latter reaction is not favored thermodynamically (endothermic by 0.38 eV on Au(111)[29] and 0.27 eV on E_7 site in this work). Maybe more importantly, the O_2 reduction via H_2O alone cannot explain (i) the removal of surface H that has been detected by experiment or (ii) the essentiality of the base addition, if O_2 can readily react with H_2O to produce OH.

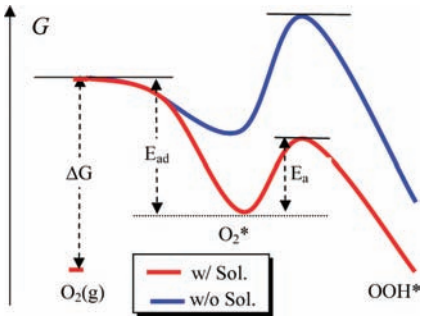

Figure 7. Simplified free energy profile of O_2 activation on Au with (red curve) and without aqueous solution (blue curve). ΔG accounts for the entropy loss for the gas phase O_2 trapping onto a surface physisorption state before its chemisorption. E_{ad} and E_a are the adsorption energy of O_2 and the reaction barrier of the O_2 + H reaction, respectively.

4. DISCUSSION

4.1. Solvation Effect on O_2 Activation. We are now at the position to address how O_2 is activated on Au nanoparticles. Our calculations show that O_2 direct hydrogenation is involved at the initial stage to produce OOH and the reaction between OOH and OH then initiates the negative charge accumulation of Au. Although the O_2 hydrogenation may not be involved at the steady state (replaced by $O_2 + H_2O \rightarrow OOH + OH$), it is critical for the activation of the whole process. Once OOH is formed, the further hydrogenation to H_2O_2 is kinetically more favorable compared to its decomposition back to O_2 and surface H. To produce OOH initially is thus the key to activate O_2, which involves two competing elementary reactions, namely, the O_2 adsorption and the O_2 hydrogenation, as illustrated in the simplified free energy profile Figure 7. At finite temperature and pressures the adsorption of gas phase molecules will experience a loss of free energy (ΔG) from the gas phase to a surface-trapped physisorption state, which is usually a large term due to the large contribution of the translational and rotational entropy. For O_2 at ambient conditions (298 K, 0.2 atm), ΔG is about 0.58 eV from standard thermodynamics data,[59] indicating a large free energy barrier for O_2 adsorption.

From Figure 7, a critical quantity for O_2 reduction is the relative order for E_{ad} and E_a. On the Au_{252} cluster, we found that $E_{ad}(O_2)$ is 0.37 eV, 0.12 eV larger than the E_a of the O_2 + H reaction (0.25 eV) in aqueous solution. This indicates that O_2 is well trapped onto the surface (long residence time) to enable the subsequent hydrogenation. By contrast, without solvent $E_{ad}(O_2)$ is only 0.17 eV, which is lower than the E_a of the O_2 + H reaction, 0.33 eV, implying that O_2 prefers to desorb instead of hydrogenation kinetically. The change in the relative order for E_{ad} and E_a can lead to a large difference in kinetics. From microkinetics with a steady-state approximation ($d[O_2{}^*]/dt = 0$), we can estimate that the O_2 reduction rate at the solid−water interface

dx.doi.org/10.1021/ja203468v | J. Am. Chem. Soc. 2011, 133, 9938–9947

is *two orders* of magnitude faster than that it at the solid−gas interface at 298 K. It is important that the presence of water solvent not only increases the residence time of O_2 on surface but also reduces the barrier of O_2 hydrogenation.

The catalytic role of water in activating O_2 on pure Au identified here can be used to explain why the water solvent is usually a must for aerobic alcohol oxidation on Au supported on inert materials at ambient conditions, such as SiO_2, activated carbon, and polymers.[8,9,54] On the other hand, in the case of the active oxide (such as TiO_2, CeO_2) supported catalysts, where the Au/active-oxide interface are known to be active for O_2 adsorption and activation,[23,60] the presence of the water solvent is no longer essential. As demonstrated in the experiment, the nonpolar solvent toluene has been widely used for aerobic oxidation on Au/active oxides.[15,19]

4.2. Structural Sensitivity of Aerobic Alcohol Oxidation. Since the α-CH bond breaking barrier of 0.71 eV at the E_7 site of Au nanoparticle is higher than that for O_2 activation, it is thus reasonable that O_2 reduction is not the rate-determining step in alcohol oxidation, although O_2 adsorption occurs dominantly at the minority edge sites of particle. By identifying the rate-determining step, it is of interest to ask whether this reaction is surface-structure sensitive. From Table 2, we can see that all reaction intermediates prefer to adsorb at the E_7 edge site of Au particle compared to the (111) surface. Among them, 1-phenylethoxy has the lowest energy cost (0.14 eV) for diffusing from the E_7 site to the (111) sites. Because other species such as O_2 prefer more strongly on the E_7 site, it is thermodynamically preferred that the phenylethoxy diffuses to the (111) terrace sites to allow for the adsorption of other species, which will lower the overall energy of the system.

To further check whether the phenylethoxy can also decompose on (111) sites, we calculated the barrier for its C−H bond cleavage on the (111) surface. The barrier is found to be 0.10 eV lower than that on the E_7 site (the located TS on (111) is shown in Figure S3 of the Supporting Information). It is therefore that the overall barrier for phenylethoxy decomposition on the (111) surface sites (diffusion plus reaction) is only 0.04 eV higher than its direct degradation on the E_7 site. This energy difference is small (∼4.7 times in rate difference at room temperature), and considering that the (111) facets are the dominant surface sites, we can deduce that the C—H bond cleavage of 1-phenylethoxy is in fact not sensitive to the surface sites on typical Au nanoparticles. The surface structure insensitivity of the alcohol oxidation reaction can explain the experimental finding by Abad et al.,[15] who showed that the rate of alcohol oxidation in Au/TiO_2 is proportional to the area of exposed Au sites.

The facile α-C—H bond breaking even on the close-packed (111) surface may not be surprising as the TS for C—H bond cleavage of 1-phenylethoxy is rather final-state-like with the evolving acetophenone being far away from the surface and the leaving H only bonding with one Au atom. From the IS to the TS, the Au surface therefore only needs to provide one atom for accepting the monovalent H, which is a classical type of surface reaction that is not sensitive to the surface sites, as demonstrated previously for CH_4 dissociation on metals.[61]

5. CONCLUSION

By mapping out the reaction network of aerobic alcohol oxidation on nano gold particles using an integrated approach based on first principles calculations and a periodic continuum solvation model, this work outlines some key features for catalytic reactions occurring on gold nanoparticles in aqueous solution. Although gold is poor in covalent bonding ability due to the saturation of its d-bands, it can still act as a good electron donor in bonding with electronegative adsorbates (similar to other transition metals). This effect of electron donation is enlarged in aqueous solution, where the solvation effect is found to enhance O_2 adsorption on gold nanoparticles dramatically due to the nonlocal polarization of the whole gold particle. We show that, without the need of minority corner or apex sites, the commonly available edge sites of Au nanoparticles are already capable to activate molecular O_2 (via hydrogenation) in an aqueous environment, which rationalizes the long-standing puzzles in the field concerning the remarkable activity difference between the liquid phase and the vapor phase for gold-based catalysis.

The most favorable reaction channel for alcohol oxidation is switched from a O_2-assisted pathway to a OH-assisted pathway with the addition of external base due to the sensitivity of the hydroxyl (alcohol) bond breaking to the basicity of the H-acceptor. In the O_2-assisted pathway, the adsorbed O_2 acts as the acceptor for the H of hydroxyl, but the reaction is still highly activated. In the OH-assisted pathway, the adsorbed OH that originates from OH anion in solution can accept easily the proton from the hydroxyl of alcohol. The consequent reaction is the same in both pathways, that is, the α-C—H bond breaking of 1-phenylethoxy. The α-C—H bond breaking can occur both at the edge and on the terrace sites of Au with the similar overall barrier (0.7 eV) due to the relatively flat potential energy surface of phenylethoxy and the intrinsic low barrier of the CH bond breaking on Au. As the α-CH bond breaking step is the rate-determining step, it is expected that the alcohol oxidation is not sensitive to the structure of typical Au nanoparticles.

The surface H produced from the α-C—H bond breaking can be removed by O_2 and OOH via a H_2O_2 pathway initially ($O_2 \rightarrow OOH \rightarrow H_2O_2$) without involving atomic O. Importantly, we also find that Au particles are negatively charged at the reaction steady state because of a facile proton-shift reaction on surface, $OOH + OH \leftrightarrow O_2 + H_2O$, which can serve as a major channel to produce OOH from O_2 by replacing the initial $O_2 + H$.

■ ASSOCIATED CONTENT

Supporting Information. Details on the implementation of CM-MPB model; methods for calculating surface energy and OH anion adsorption free energy; model of Au(322) slab; optimized structures for TS structures of O_2 dissociation, TS6, TS7, $OOH + OH$, and $O_2 + H_2O$; and TS for α-CH dehydrogenation on Au(111). This material is available free of charge via the Internet at http://pubs.acs.org.

■ AUTHOR INFORMATION

Corresponding Author
zpliu@fudan.edu.cn

■ ACKNOWLEDGMENT

This work is supported by the National Nature Science Foundation (NSF) of China (20825311), 973 program (2011CB808500), Science and Technology Commission of Shanghai Municipality (08DZ2270500), and Program for

Professor of Special Appointment (Eastern Scholar) at Shanghai Institute of Higher Learning.

REFERENCES

(1) Sheldon, R. A.; Dakka, J. *Catal. Today* **1994**, *19*, 215–245.
(2) Gallezot, P. *Catal. Today* **1997**, *37*, 405–418.
(3) Prati, L.; Rossi, M. *J. Catal.* **1998**, *176*, 552–560.
(4) Besson, M.; Gallezot, P. *Catal. Today* **2000**, *57*, 127–141.
(5) Corma, A.; Garcia, H. *Chem. Soc. Rev.* **2008**, *37*, 2096–2126.
(6) Comotti, M.; Della Pina, C.; Falletta, E.; Rossi, M. *Adv. Synth. Catal.* **2006**, *348*, 313–316.
(7) Zhu, J. J.; Figueiredo, J. L.; Faria, J. L. *Catal. Commun.* **2008**, *9*, 2395–2397.
(8) Tsunoyama, H.; Ichikuni, N.; Sakurai, H.; Tsukuda, T. *J. Am. Chem. Soc.* **2009**, *131*, 7086–7093.
(9) Lucchesi, C.; Inasaki, T.; Miyamura, H.; Matsubara, R.; Kobayashi, S. *Adv. Synth. Catal.* **2008**, *350*, 1996–2000.
(10) Villa, A.; Janjic, N.; Spontoni, P.; Wang, D.; Su, D. S.; Prati, L. *Appl. Catal., A* **2009**, *364*, 221–228.
(11) Guan, Y. J.; Hensen, E. J. M. *Appl. Catal., A* **2009**, *361*, 49–56.
(12) Carrettin, S.; Concepcion, P.; Corma, A.; Nieto, J. M. L.; Puntes, V. F. *Angew. Chem., Int. Ed.* **2004**, *43*, 2538–2540.
(13) Date, M.; Okumura, M.; Tsubota, S.; Haruta, M. *Angew. Chem., Int. Ed.* **2004**, *43*, 2129–2132.
(14) Wang, C. M.; Fan, K. N.; Liu, Z. P. *J. Am. Chem. Soc.* **2007**, *129*, 2642–2647.
(15) Abad, A.; Corma, A.; Garcia, H. *Chem.—Eur. J.* **2008**, *14*, 212–222.
(16) Mallat, T.; Baiker, A. *Chem. Rev.* **2004**, *104*, 3037–3058.
(17) Conte, M.; Miyamura, H.; Kobayashi, S.; Chechik, V. *J. Am. Chem. Soc.* **2009**, *131*, 7189–7196.
(18) Haider, P.; Kimmerle, B.; Krumeich, F.; Kleist, W.; Grunwaldt, J. D.; Baiker, A. *Catal. Lett.* **2008**, *125*, 169–176.
(19) Mitsudome, T.; Noujima, A.; Mizugaki, T.; Jitsukawa, K.; Kaneda, K. *Adv. Synth. Catal.* **2009**, *351*, 1890–1896.
(20) Zheng, N.; Stucky, G. D. *Chem. Commun.* **2007**, 3862–3864.
(21) Shang, C.; Liu, Z. P. *J. Phys. Chem. C* **2010**, *114*, 16989–16995.
(22) Yang, J.; Guan, Y. J.; Verhoeven, T.; van Santen, R.; Li, C.; Hensen, E. J. M. *Green Chem.* **2009**, *11*, 322–325.
(23) Liu, Z. P.; Gong, X. Q.; Kohanoff, J.; Sanchez, C.; Hu, P. *Phys. Rev. Lett.* **2003**, *91*, 266102.
(24) Jorgensen, B.; Christiansen, S. E.; Thomsen, M. L. D.; Christensen, C. H. *J. Catal.* **2007**, *251*, 332–337.
(25) Gong, J. L.; Mullins, C. B. *J. Am. Chem. Soc.* **2008**, *130*, 16458.
(26) Liu, Z. P.; Hu, P.; Alavi, A. *J. Am. Chem. Soc.* **2002**, *124*, 14770–14779.
(27) Wittstock, A.; Neumann, B.; Schaefer, A.; Dumbuya, K.; Kubel, C.; Biener, M. M.; Zielasek, V.; Steinruck, H. P.; Gottfried, J. M.; Biener, J.; Hamza, A.; Baumer, M. *J. Phys. Chem. C* **2009**, *113*, 5593–5600.
(28) Meyer, R.; Lemire, C.; Shaikhutdinov, S. K.; Freund, H. *Gold Bull.* **2004**, *37*, 72.
(29) Zope, B. N.; Hibbitts, D. D.; Neurock, M.; Davis, R. J. *Science* **2010**, *330*, 74–78.
(30) Yang, X. M.; Wang, X. N.; Liang, C. H.; Su, W. G.; Wang, C.; Feng, Z. C.; Li, C.; Qiu, J. S. *Catal. Commun.* **2008**, *9*, 2278–2281.
(31) Yan, T.; Gong, J.; Mullins, C. B. *J. Am. Chem. Soc.* **2009**, *131*, 16189–16194.
(32) Wang, H. F.; Liu, Z. P. *J. Phys. Chem. C* **2009**, *113*, 17502–17508.
(33) Li, Y. F.; Liu, Z. P.; Liu, L. L.; Gao, W. G. *J. Am. Chem. Soc.* **2010**, *132*, 13008–13015.
(34) Fang, Y. H.; Liu, Z. P. *J. Am. Chem. Soc.* **2010**, *132*, 18214–18222.
(35) Soler, J. M.; Artacho, E.; Gale, J. D.; Garcia, A.; Junquera, J.; Ordejon, P.; Sanchez-Portal, D. *J. Phys.: Condens. Matter* **2002**, *14*, 2745–2779.
(36) Troullier, N.; Martins, J. L. *Phys. Rev. B: Condens. Matter* **1991**, *43*, 1993–2006.
(37) Junquera, J.; Paz, O.; Sanchez-Portal, D.; Artacho, E. *Phys. Rev. B: Condens. Matter* **2001**, *64*, 235111.
(38) Perdew, J. P.; Burke, K.; Ernzerhof, M. *Phys. Rev. Lett.* **1996**, *77*, 3865–3868.
(39) Anglada, E.; Soler, J. M.; Junquera, J.; Artacho, E. *Phys. Rev. B: Condens. Matter* **2002**, *66*, 205101.
(40) Garcia-Gil, S.; Garcia, A.; Lorente, N.; Ordejon, P. *Phys. Rev. B: Condens. Matter* 2009, *79*, 075441.
(41) Wang, H. F.; Liu, Z. P. *J. Am. Chem. Soc.* **2008**, *130*, 10996–11004.
(42) Shang, C.; Liu, Z. P. *J. Chem. Theory Comput.* **2010**, *6*, 1136–1144.
(43) Hamm, U. W.; Kramer, D.; Zhai, R. S.; Kolb, D. M. *J. Electroanal. Chem.* **1996**, *414*, 85–89.
(44) Wulff, G. Z. *Kristallogr. Mineral.* **1901**, *34*, 449–530.
(45) Cerf, R. In *Wulff Crystal in Ising and Percolation Models*, 1st ed.; Springer: New York, 2006; Vol. 1878.
(46) Jirkovsky, J. S.; Halasa, M.; Schiffrin, D. J. *Phys. Chem. Chem. Phys.* **2010**, *12*, 8042–8052.
(47) Cleveland, C. L.; Landman, U.; Schaaff, T. G.; Shafigullin, M. N.; Stephens, P. W.; Whetten, R. L. *Phys. Rev. Lett.* **1997**, *79*, 1873–1876.
(48) Gao, Y.; Shao, N.; Zeng, X. C. *ACS Nano* **2008**, *2*, 1497–1503.
(49) Seo, D.; Yoo, C. I.; Park, J. C.; Park, S. M.; Ryu, S.; Song, H. *Angew. Chem., Int. Ed.* **2008**, *47*, 763–767.
(50) Liu, X. G.; Wu, N. Q.; Wunsch, B. H.; Barsotti, R. J.; Stellacci, F. *Small* **2006**, *2*, 1046–1050.
(51) Grzelczak, M.; Perez-Juste, J.; Mulvaney, P.; Liz-Marzan, L. M. *Chem. Soc. Rev.* **2008**, *37*, 1783–1791.
(52) Valden, M.; Lai, X.; Goodman, D. W. *Science* **1998**, *281*, 1647–1650.
(53) Tsunoyama, H.; Sakurai, H.; Tsukuda, T. *Chem. Phys. Lett.* **2006**, *429*, 528–532.
(54) Sun, K. Q.; Luo, S. W.; Xu, N.; Xu, B. Q. *Catal. Lett.* **2008**, *124*, 238–242.
(55) Xu, Y.; Mavrikakis, M. *J. Phys. Chem. B* **2003**, *107*, 9298–9307.
(56) Boronat, M.; Corma, A. *Dalton Trans.* **2010**, *39*, 8538–8546.
(57) Kelly, C. P.; Cramer, C. J.; Truhlar, D. G. *J. Chem. Theory Comput.* **2005**, *1*, 1133–1152.
(58) Palascak, M. W.; Shields, G. C. *J. Phys. Chem. A* **2004**, *108*, 3692–3694.
(59) *CRC Handbook of Chemistry and Physics*, 84th ed.; CRC Press: Boca Raton, FL, 2003−2004.
(60) Venezia, A. M.; Pantaleo, G.; Longo, A.; Di Carlo, G.; Casaletto, M. P.; Liotta, F. L.; Deganello, G. *J. Phys. Chem. B* **2005**, *109*, 2821–2827.
(61) Liu, Z. P.; Hu, P. *J. Am. Chem. Soc.* **2003**, *125*, 1958–1967.